Progress on the Coherent Beam Recombination project

Contact *marco.galimberti@stfc.ac.uk*

N. Martin, W.H. Fraser, V. C. Lindsay, B. Parry, M. Galimberti

Central Laser Facility, STFC Rutherford Appleton Laboratory, OX11 0QX, UK

Introduction

The coherent beam recombination is a possible solution to overcome the current limitation on the maximum achievable power of the high power laser system.

HAPPIE lab project is devoted to investigate this technique. In order to achieve this, all the beams must be spatially and temporally locked to each-other, and also must be of the same path length to the precision of fraction of a micrometre. The progress of the work to achieve this are listed in this report and with also the preliminary results.

The project this year builds on the previous work of placement students, most notably in the last two years where Victoria Lindsay achieved spatial stabilisation and Will Fraser achieved temporal stabilisation. As coherent combination has effectively been achieved, the project this year focused on optimising the system. In particular, three main areas were focused on:

1. Changing the mounting method of the piezo mirror which stabilises the beam spatially and temporally. The current setup caused aberrations to the far field, most notably astigmatism.
2. Developing a low cost PID control system for spatial stabilisation using Red Pitayas, offering an alternative to the expensive analogue SIM modules.
3. Developing an easy method to ensure the difference in path length traversed by the two lasers is within the coherence length so that constructive interference can occur with non-CW lasers

Theory

Coherent Beam Combination

If two lasers beams are incident on the same point and, if they are pulsed, at the same time, the electric fields of the lasers constructively interfere with one another and interference fringes are produced at that point.

The electric fields of two lasers travelling in free space can be described by the generalised equations:

$$\vec{E}_1 = \vec{E}_{01} e^{i(\vec{k}_1 \vec{r} - wt + \theta_1)} \quad [1]$$

$$\vec{E}_2 = \vec{E}_{02} e^{i(\vec{k}_2 \vec{r} - wt + \theta_2)} \quad [2]$$

where ω is the angular frequency, k_1 and k_2 are the respective wave numbers and θ_1 and θ_2 are the respective phases.

If the electric fields were to overlap with each other spatially and temporally (with also the same polarization), they superimpose, so that the resulting electric field is the sum of the two electric fields combined:

$$\vec{E}_{total} = \vec{E}_1 + \vec{E}_2 = \left(\vec{E}_{01} e^{(\vec{k}_1 \vec{r} + \theta_1)} + \vec{E}_{02} e^{i(\vec{k}_2 \vec{r} + \theta_2)}\right) e^{-i\omega t} \quad [3]$$

The intensity of the resulting field is equal to modulus squared:

$$I_{total} = \langle \left| \vec{E} \right|^2 \rangle = \langle \vec{E} \,.\, \vec{E}_* \rangle \quad [4]$$

Substituting in the expressions for the electric fields we find

$$I_{total} = I_1 + I_2 + 2\sqrt{I_1 I_2} cos\phi \quad [5]$$

where ϕ is the phase difference between the two waves. If the two electric fields have equal intensities and the phase difference is equal to zero, then the equation can be simplified to be:

$$I_{total} = 4I \quad [6]$$

A generalised derivation that instead of two beams has *N* beams constructively interfering with one another can show that the intensity of the resulting field scales proportionally with the square of the number of beams: [1]

$$I_{total} = N^2 I \quad [7]$$

PID Control and Filtering

To achieve spatial and temporal stabilisation, a PID control system is employed which can be used to drive a mirror. This corrects the jitter in the far field that is caused by thermal fluctuations.

The PID control system is named after the three components which determine the output: Proportional, Integral and Derivative. As shown by equation *8*, by measuring during a time τ the integral swept by the error e (the difference between the desired set-point and measured value), the PID coefficients (k_p, k_i, k_d) can be tuned so that they output a correction that leads to a high stable configuration. [2]

$$u(t) = k_p \left(e(t) + k_i \int_0^t e(\tau) d\tau + k_d \frac{de(t)}{dt} \right) \quad [8]$$

To tune the parameters, a known slow but stable PID configuration is setup and an output frequency sweep oscillates the desired set point so to measure how well the system responds at different frequencies. It is therefore useful to use the Fourier transform of equation *8*

$$u(\omega) = k_p e(\omega) \left(1 - \frac{i k_i}{\omega} + k_d i\omega\right) \quad [9]$$

to be able to tune the parameters as the frequencies used in the sweep can easily converted into angular frequencies. An offset can also be added to equations *8* and *9* if required.

An additional parameter that can be added to increase the speed of the stabilisation is a low-pass Butterworth filter. This is added before the signal is passed to the PID control system so that high frequencies are not corrected for. This is simply because the mirror the PID loop is outputted to will not be able to oscillate fast enough to correct high frequencies, leading to instabilities.

A Butterworth filter is specifically chosen because it has the flattest response curve of any filter. This is useful as we want to minimise the response of high frequencies as much as possible. The response curve is determined by equation *10* and shown by *Figure 3*[3]:

$$F(x) = \frac{1}{1 + x^n} \quad [10]$$

By adding filters together in a linear combination, various orders can be achieved that provide different flatness responses at the cut-off frequency.

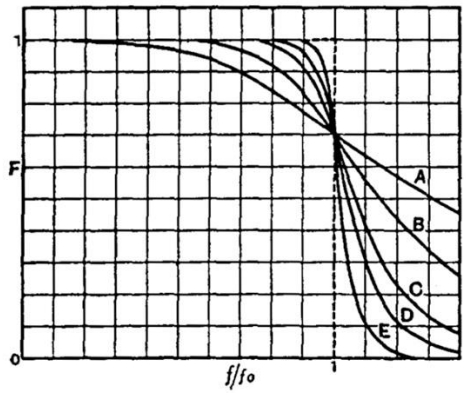

Figure 3: *Response Curve of a Butterworth Filter. The various curves show the flatness of different order filters where 'A' is the lowest order and 'E' is the highest order.*

Red Pitayas

The Red Pitaya is a cheap and affordable field-programmable gate array (FPGA) that contains two RF inputs and two RF outputs (both 125MS/s). It also has a 50MHz analogue bandwidth and 14-bit analogue-to-digital and digital-to-analogue converters. The boards are intended as an alternative to expensive laboratory measurement and control systems.

FPGAs are not a relatively new industry, with the first being produced in 1984 by Altera. Due to improvements in computing power, they have recently begun being used often in the laboratory with the Red Pitaya Company being established in 2013. FPGAs are characterised as integrated circuits, where large numbers of transistors can act as programmable logic blocks. A hierarchy of reconfigurable interconnects between the logic blocks allow for flexible reconfigurable computing. This allows Red Pitayas to be suitable for PID control systems, and can additionally perform fast low-pass, high-pass and band-pass filtering. [4]

FPGA PID Control and Filtering

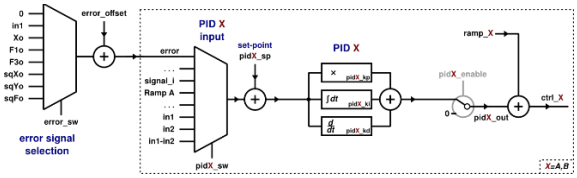

Figure 4: *Schematic of the Red Pitaya PID Loop written by Marcelo Luda. The figure includes additional features available, such as a ramp, that are not currently used for the HAPPIE project.*

For an input signal denoted as *in* and the set-point as *sp*, the output is given by:

$$out = k_p \cdot (sp - in) + k_i \cdot \int_0^t (sp - in)dt + \\ + kd \cdot \frac{d}{dt}(sp - in) \qquad [11]$$

with adjustable PID coefficients $k_p = \frac{PIDX\_kp}{scale}$, $k_i = \frac{PIDX\_ki}{t_i}$, $k_d = \frac{PIDX\_kd}{\tau_d}$. Here the PIDX value is continuously adjustable, although the scale values are discrete. For the proportional value, this can allow a large array of values. For the integral element, k_i can be varied either by the scaling parameter, *PIDX_ki*, or by changing a scale of the integrator time τ_i which relates to the characteristic time τ such that: $\tau = \frac{\tau_i}{pidX\_ki}$. In a similar manner, the derivative term can also be adjusted [5]

Temporal Locking

For the two beams to produce interference fringes, they must overlap each other temporally. This has been easily achieved by previous students by moving a delay arm from one of the beams in steps less the coherence length until an interference pattern appears on a camera. The maximum difference between the two arms where interference fringes are still observed is known as the coherence length, L_{coh} , defined by [6]:

$$L_{coh} = \frac{c}{\Delta v} = c\tau_{coh} \qquad [12]$$

where c is the speed of light, Δv is the frequency bandwidth and τ_{coh} is the coherence time.

Spectral Interferometry

If the two beams are both inputted to a spectrometer, not necessarily temporally overlapped, but with a time delay between the pulses, τ, the combined optical spectrum can be recorded. If the electric field of the two pulses are described by phasors, $E_1(\omega)$ and $E_2(\omega)$, the time delay equates a phase factor $\exp(-i\omega\tau)$. The combined electric field can be written as

$$E(\omega) = E_1(\omega) + E_2(\omega)\exp(-i\omega\tau) \qquad [13]$$

which modulates the optical spectrum, causing an oscillation with phase

$$\varphi(\omega) = \omega\tau + \varphi_1(\omega) - \varphi_2(\omega) \qquad [14]$$

If the time delay is too great, the phase will oscillate too quickly for the spectrometer to detect, making it indistinguishable from noise. [7]

Method

Layout

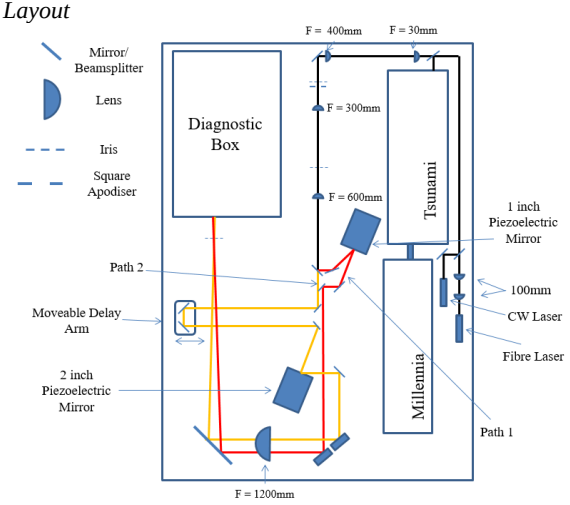

Figure 5: *Schematic of the HAPPIE Lab Layout before reaching the diagnostic area. The Millennia and Tsunami are currently broken and are due for replacement within the next year.*

An 808nm CW laser and a single mode broad-bandwidth fibre 1050nm laser both traverse around the setup as shown in *figure 5*. The single mode fibre additionally goes through a telescope to help correct for chromatic aberration that occurs between the two lasers. Both firstly travel through a telescope before passing through a square apodiser. The beams travel through another telescope to ensure relay imaging of the apodiser before hitting a 50:50 beam splitter. On one path (path 2 in *figure 5*), the beam

hits a two inch mirror attached to a two inch platform via a screwed in cross-mount that contains three steel pins, as shown by *figure 6*. Three magnets are superglued to the mirror in the same formation as the cross-mount so that the magnetic attraction between the pins and magnets hold the mirror to the mount. The platform is connected to piezo driver that can perform fast spatial stabilisation (in directions of X and Y). On the other path, the beam hits a thin two inch mirror which is attached to a one inch platform. The mechanism to attach the mirror to the platform is the same. This platform is also connected to a piezo driver which is able to perform spatial and temporal stabilisation (in directions X, Y and Z).

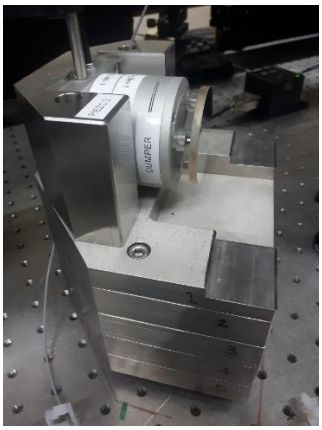

Figure 6: *Mounting Mechanism for the correcting mirror. Shown is the two inch mount, with the one inch mount also using the same mechanism.*

The beams then travel onto two mirrors alongside each other, which are can be controlled by picomotors. With the beams now propagating next to each other, they go through a *1200mm* lens and are focused through an iris into a black box. It is here that the measurements of the near-field and far-field are taken, so they are enclosed inside the black box to reduce noise caused by air flow from the air conditioning in the room.

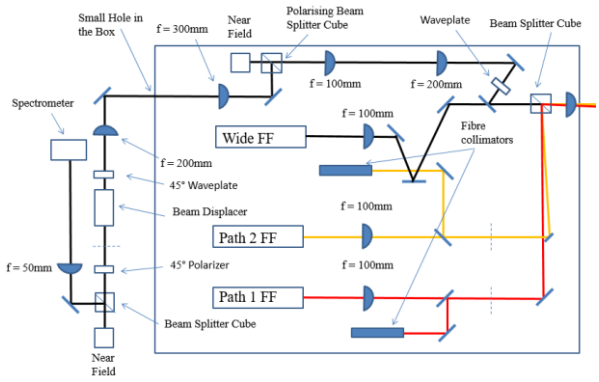

Figure 7: *Layout inside the diagnostic box and also further diagnostics outside it. The figure continues on from figure 5, with the beam approaching from the right.*

The layout inside the black box is showed by *figure 7*. The beams travel through a collimating lens before hitting a beam splitting cube.
On the arm that travels left, far-field measurements are taken of the two beams using PSDs whose signal is then used to feed the spatial stabilisation. 10% of each beam is additionally sent to a camera. This allows for a reference to be set where the PSD measures a central position. The picomotors earlier in the system can direction the beam onto this reference if it drifts.
On the arm that travels straight through the cube, the beam travels through a high pass filter so that the CW is fully attenuated and the single mode fibre passes undisturbed. The beams then hit a further 50:50 mirror. The beams that travel through are then measured on a wide far-field. It here that both beams are overlapped so constructive interference can occur. On the other arm, the beams travel through a waveplate, and a telescope (again to ensure relay imaging). It then hits a polarising cube, splitting the beam with a minimal amount going to a near-field camera and the rest travelling out of the black box, which is then used to help estimate the difference in path length between the arms. The purpose of the waveplate earlier is to control the amount of the beam is sent to the near-field camera.

Spatial Stabilisation

Each PSD far-field output is connected to a SIM module which contains a low-pass Butterworth filter and a PID module. This is then outputted to a piezo driver, which corrects the relevant mirror to stabilise the far-field.
To achieve fast spatial stabilisation, the value and order of the low-pass filter as well as the values of the P, I and D coefficients must be optimised. This could be done manually by observing the fluctuations in the recorded position in X and Y when changing the parameters. However, this process is slow and inefficient. In addition, the D coefficient cannot be optimised in this way.
Instead, values are first chosen which produce a slow but a stable stabilisation. Typically, these values are P = ±1, I = 10, D = 0 with a second order low pass filter with a cut-off of 5Hz. A lock-in amplifier then performs a frequency sweep that oscillates the set-point that the PID loop aims to adjust to. With the slow spatial stabilisation on, the PSD output amplitude and phase values are recorded for each frequency. An example of this is shown by *figure 8*. The graph can be interpreted as a measure of the resonances of the mirror and mount and this data can be used to fine-tune the PID parameters to keep up well with these resonances, or to disregard them by using the low-pass filter.

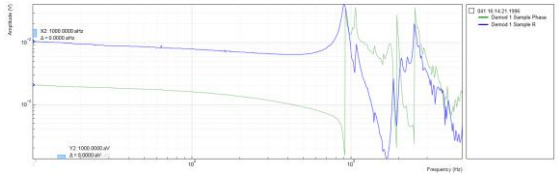

Figure 8: *Closed loop frequency sweep using slow-response PID coefficients. The graph shows a resonance of the platform and mirror at approximately 900Hz.*

To optimise the values, a Monte-Carlo simulation is run that uses repeated random sampling. The code works by simulating the closed loop frequency sweep curve for a very large combination of values of P, I and D, and using the open loop to predict which values would lead to the least over-shooting for natural resonances. If this process is repeated for each axis for both mirrors, full spatial stabilisation can be achieved.
Alternatively, instead of using SIM Modules, Red Pitayas could also be used to perform the control loop. As they have two inputs and two outputs, one red pitaya can be used to perform a low-pass filter for both the X and Y input. These are connected to another Red Pitaya which performs the PID control loop. Unfortunately, the software to perform all of this on a single Red Pitaya does not currently exist.
The software used to perform a low-pass filter is called *Pyrpl*. We use the so-called PID module, although the derivative function does not work currently and it is effectively a PI module. The input filter only allows discrete values which are in powers of two. The proportional coefficient is set to 1 so that there is an output signal without further correcting the signal. This was tested with no filter to ensure that it fully recreated the input signal. We also used a frequency sweep from the lock-in amplifier as an input to a PID with P = 1 and filters of various magnitudes and orders to test that the filters were accurate.

The signal is then passed to the second Red Pitaya which performs the PID control loop. The software which performs this is written by Marcelo Luda and is called Lock-in PID.

Temporal Stabilisation

If the two beams paths lengths are the same to within the coherence length, then interference fringes are produced. However, due to thermal fluctuations, the beam path lengths will not stay perfectly the same, or even stay within the coherence length. They therefore need to be locked using another PID control system. This was developed last year by Will Fraser and, just like the spatial stabilisation, uses the CW laser.

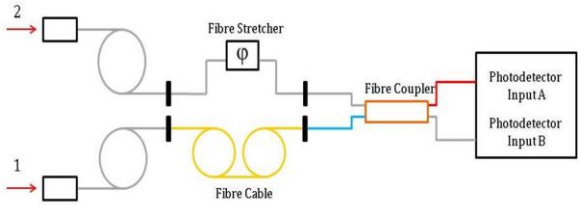

Figure 9: *Schematic of the layout used to achieve the temporal stabilisation.*

As shown by *Figure 9*, the CW travels into a fibre collimator on each beam path. If they are aligned well, one arm travels through some fibre cable and the other into a fibre stretcher. Applying a voltage to the fibre stretcher allows the path length to change, and therefore the phase. Both arms then connect to a fibre coupler, which then outputs an RF signal given by:

$$RF(t) = A\sin\left(\frac{2\pi}{\lambda}D(t) + \phi(t)\right) \qquad [15]$$

where $\phi(t)$ is the phase difference in time between the two arms, $D(t)$ is the delay and A is a constant.

The outputted RF signal is then inputted to a PID unit which outputs to the fibre stretcher to stabilise the phase. However, to achieve temporal stabilisation a further PID control loop is required that takes the input to fibre stretcher and outputs to the one inch platform that mounts the thin two inch mirror. The reason why two PID loops are required here is because the mirror is unable to adjust fast enough for sudden vibrations like doors banging. If only one loop was to be used, events like this would cause the loop to run out of range. In contrast, the lack of mechanical components with the first PID loop means that is able to stabilise these disturbances without running out of range. The process to obtain stable and fast PID coefficients and filter values is the same as for the spatial stabilisation tuning.

Ensuring Equal Path Length

Returning to the layout, we now look at the beam that exits the black box (after just being split by a polarising cube), as shown by *Figure 7*.

The beam travels through an additionally telescope, so that the near-field as shown on the camera is relay imaged. The beams then travel through a waveplate that rotates the polarisation by 45° so that they are equally s-polarized and p-polarized.

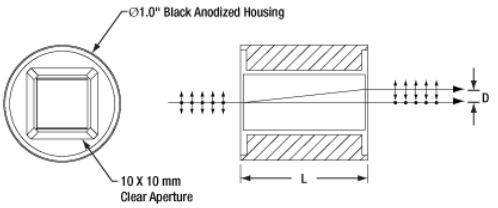

Figure 10: Schematic and Ray Diagram of Mounted Calcite Beam Displacer [8]

They then travel through a calcite beam displacer as shown in *figure 10*. This splits each beam by their polarisation, so an additional two beams are produced which propagate in the same plane. The setup can then be aligned so that two middle beams overlap each other. It is these two overlapped beams that are of interest so an iris stops the other beams. As they are of opposite polarisation, they travel through a polarizer that is halfway between the two polarization states, so that both beams are attenuated by 50%. A 10:90 beam splitting cube allows the beam to be imaged onto a camera, through the weaker arm, to optimise these components. The stronger arm then is focused with a lens. However, crucially, before the beam becomes diffraction-limited, it enters into a spectrometer so that it doesn't integrate over the entire spectrum. If the beams are well aligned and the two beams path lengths are the same to an accuracy of about 1cm, an interference pattern will form in the spectrum.

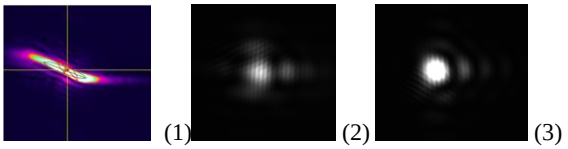
(1) (2) (3)

Figure 11: *CW far-fields (1) using previous mounting mechanism, (2) of Path 1 with the new mounting mechanism, (3) Path 2 using the new mounting mechanism.*

Results

Figure 11 shows the far-fields of the two arms and also the far-field using the previous mounting mechanism. On path 1, the far-field shows a small amount of astigmatism. The lens has been positioned to minimise the astigmatism in either direction, resulting in the characteristic cross pattern. On path 2, no astigmatism is present and the spots appears brighter. The far-field exhibits a small amount of coma (there is also a small degree of this on path 1). The quality of the focal spots is a dramatic improvement to the previous heavily astigmatised far-fields, caused by the gluing of the mirrors to the platforms.

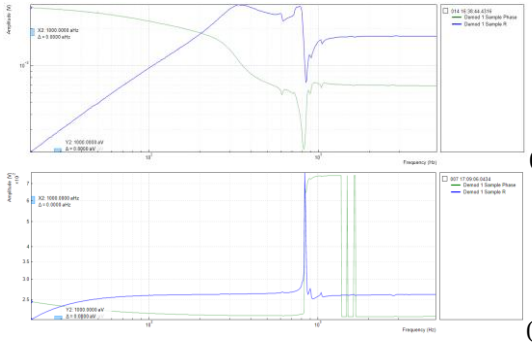
(1)

(2)

Figure 12: *Closed loop curves of the X-component of the mirror on the one inch platform. Plotted against frequency is the amplitude of the oscillation (in blue) and phase (in green). (1) Shows the curve using the analogue SIM module with finely tuned parameters and (2) shows the curve using the Red Pitayas using manually tuned parameters.*

Figure 12 shows how effective the Monte-Carlo code is at tuning the parameters. The curve produced by the SIM module shows a moderate overshoot in the region of *400-900Hz*. However, using the Red Pitayas, during the resonance between *800-900Hz*, initially shown by *figure 8* in the open loop scan, the control system massively overshoots and is unable to effectively manage it.

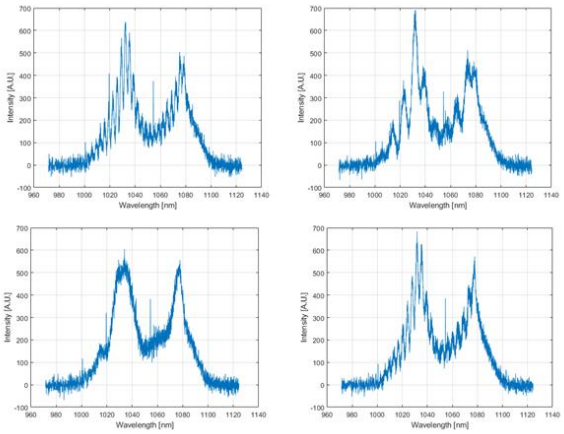

Figure 13: *Spectrometer when delay arm is 24.34mm, 24.24mm, 24.14mm and 24.04mm*

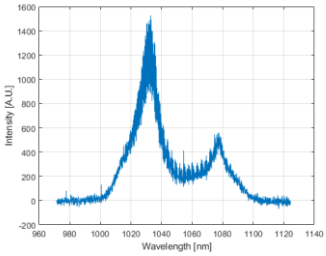

Figure 14: *Spectrometer when delay arm is 22.92mm. At this distance, fringes are shown on the WFF.*

Figure 13 shows the interference pattern created in the spectrometer when the two beams are spatially overlapping and close to being temporally overlapped.

Various interference patterns are shown for difference delay values (note that the real delay length is double the delay arm value). As expected, even small changes in the scale of *100µm* can cause large changes in the pattern. It was found that the coherence length for the fringes in the spectrometer was approximately *10mm.* For the relatively small system the HAPPIE lab uses, that gives a reasonable range to find the temporal overlap on the cameras, without making it too difficult to find on the spectrometer. However, for a larger system like Vulcan, this could much more difficult.

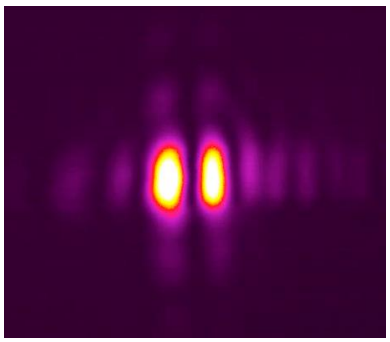

Figure 15: *Combined WFF of two spatially and temporally overlapping beams from the single mode broad-bandwidth fibre 1050nm laser, of each path length accurate to one micron.*

It was expected that interference on the cameras would occur when the fringes on the spectrometer were maximally wide, as demonstrated by *equation 14*. However, *figure 14* shows the spectrometer fringes when interference fringes appeared on the camera, shown by *figure 15*. In reality, these fringes are so narrow that they are hard to distinguish from the signal noise.

Discussion

Figure 11 shows that the quality of the focal spot has dramatically improved with the new three pin magnetic method of mounting the mirror. Previously, the mirrors were glued onto the mount, which caused lots of astigmatism. On the path with the two inch mirror mount, no astigmatism is observed with the main aberration present being coma. However, on the path with the one inch mirror mount, astigmatism is still present. Other than the size of the platforms, the main difference is the thickness of the mirrors. The mirror on the one inch path is significantly thinner so that its reduced inertia allows it to perform a quicker temporal stabilisation. If the system were to be used only for spatial stabilisation, as has been proposed, further investigation is required to determine if a thin mirror on a two inch platform performs better.

Frustratingly, since changing the mirrors, the temporal stabilisation is considerably slower and less stable. If this were to be studied, it is expected that increasing the thickness of the mirror would reduce the astigmatism but reduce the speed of the temporal stabilisation. Whether the current setup is an acceptable trade-off remains to be seen. Currently, the instabilities in the temporal stabilisation cause some instabilities in the spatial stabilisation. It has been found that increasing the gain (by a factor of four) on the spatial stabilisation can help account for this. However, even at optimum stability, vibrations such as doors banging were enough to destabilise the system to the point that it couldn't recover. This was because the PID system cannot react fast enough, so it runs out of range before it can.

As mentioned, previously the one inch platform had a one inch mirror mounted onto it. As the beam being stabilised is a 1cm square, a 1:1 telescope was placed around the mirror, so that the beam was focused onto it. The telescope was collimated using the CW laser and a shear plate. However, due to chromatic aberration, it was found that the two beams did not focus at the same focal length in the wide far-field. This problem had been previously undetected due to the distortions of the correcting mirrors.

Progress with the Red Pitayas presents a lot of promise that cheap spatial stabilisation can soon be achieved throughout Vulcan and other large laser systems and their programmable nature means they will be easy to incorporate. Even though the PID coefficients were not tuned, they were able to halve the jitter caused by thermal fluctuations and it is hoped that once software for the tuning is developed, stabilisation similar to that of the analogue SIM modules could be achieved. However, the digital low-pass filter used in the pyrpl software only allowed cut-off frequencies that are a power of two. This allows significantly less scope for fine-tuning and could prove to be a stumbling-block for the digital control loop. The problem arises because FPGAs work with binary data to process real-time operations (at least for feedback applications, where is critical to have a short IN-OUT response time). To make a filter, a division has to be made. However, that division cannot happen without an algorithm (aka: step-by-step procedure that is not-real time) unless it is a power of two division. In the next year, it will be investigated whether it is possible to make our own filters in Verilog that will be able to perform low-pass filtering with a far greater range of cut-off points, which can also work in real-time operations. In addition it will be investigated whether we are able to write a combined software, which is able to perform by digital filtering and PID.

The next step will be to modify the Monte-Carlo simulation code so that only the discrete low-pass filter values allowed on the *pyrpl* software can be simulated. Once this is done, the Red

Pitaya PID coefficients can be tuned and it can be investigated how fast a spatial stabilisation can be achieved. It may be that it is good enough to completely replace the Sim Modules. However, due to the discretized filter values, it is likely to be not as fast, and although maybe good for general spatial stabilisation, it is suspected that it will be not good enough for coherent combination. Currently with manual tuning, it is not nearly good enough to be able to be combined with temporal stabilisation.

Applying the spectrometer to give an initial estimate of how close the paths are to equal length worked relatively well. When fringes first appeared on the spectrometer, the path difference was approximately one centimetre away from the coherence length. It was expected that fringes would appear on the camera when the fringe on the spectrometer were broadest. However, this did not occur as shown by *Figure 14*. Instead, they occurred at approximately 2.64mm of further delay. After some investigation, it was found that the cause of this was the calcite beam displacer. Considering the refractive index and the geometry of the path traversed, we calculated a figure for the additional discrepancy of the path lengths of the two arms which closely matched the recorded figure. Armed with this knowledge, this can make the difficult task of ensuring equal path length easier. Future steps will be taken next year to see if an interferometry setup could further improve this setup.

It is expected that two further temporal control loops will be required to perfect the setup. It was observed that even when both the spatial and temporal stabilisation was running, the fringe intensities would slowly drift. This is because the mirror which performs the temporal stabilisation slowly moves in one direction and runs out of range after approximately twenty minutes. By measuring the intensity centroid of the fringes, a further control loop can be added that outputs to the set-point of the second temporal PID loop. An additional mirror can also be added that performs a slow temporal stabilisation but has a much larger range. Something also to consider is that the quality of the fringes degraded rapidly with time. Even a change of path difference of a couple of microns (which can happen over the course of an hour due to thermal fluctuations) can causes this, and leaving the laser system off for over a week can lose the fringes entirely.

Conclusion

Developments this year in the HAPPIE lab mean that, along with previous years of work, coherent combination of two high power femtosecond lasers is close to becoming a reality in the lab. The key problem of mounting the mirrors which perform the stabilisation without causing aberrations has been solved. Additionally, there is now an easy way to ensure that the difference between the beam paths is less than the coherence length, so that constructive inference can occur in non-CW lasers. It has yet to be seen whether the Red Pitayas can provide a control system as fast as the analogue SIM Modules as there is no current method to tune the parameters. However, it is likely that they will be suitable for general beam stabilisation in Vulcan and Gemini due to their affordability and also effectiveness when just performing manual tuning.

References

1. P.Hariharan, Basics of Interferometry, 2nd Edition, Academic press, 2006.
2. PID Control, California Institute of Technology
3. S. Butterworth, *On the Theory of Filter Amplifiers*, Experimental Wireless, 1930
4. Red Pitaya < https://www.redpitaya.com/>
5. Lock-In+PID < https://marceluda.github.io/rp_lock-in_pid/>
6. E. Hecht, Optics, Fifth Edition, Pearson, 2017
7. RP Photonics – Spectral Phase Interferometry. < https://www.rp-photonics.com/spectral_phase.html>
8. Thorlabs – Mounted Calcite Beam Displacer. https://www.thorlabs.com/NewGroupPage9.cfm?ObjectGroup_ID=745